Research Article Vol. 1, No. 4 / 15 Apr 2022 / Optics Continuum 623
OPTICS CONTINUUM

Ultra-compact wideband filter with sidelobe suppression based on double modulated grating-assisted microring resonator

CHUANQI FANG,[1] VIVEK RAJ SHRESTHA,[2] IKECHI AUGUSTINE UKAEGBU,[3] GUANGHUI REN,[4] SHILONG PAN,[1,5] AND BIKASH NAKARMI[1,6]

[1]College of Electronic and Information Engineering, Nanjing University of Aeronautics and Astronautics, Nanjing, 211106, China
[2]School of Physics, The University of Melbourne, VIC 3010, Australia
[3]School of Engineering and Digital Sciences, Nazarbayev University, 53 Kabanbay Batyr Avenue, 010000 Nur-Sultan, Kazakhstan
[4]Integrated Photonics and Applications Center (InPAC), School of Engineering, RMIT University, Melbourne, VIC 3001, Australia
[5]pans@nuaa.edu.cn
[6]bikash@nuaa.edu.cn

Abstract: In this paper, we propose an ultra-compact wideband filter (WBF) with high sidelobe suppression. The filter consists of a single microring resonator incorporated with a proposed new structure of double modulated subwavelength gratings. The double modulated subwavelength gratings are obtained via two different fill factors with the same period. The ultra-compact WBF achieved FSR-free, flat response with a 3 dB bandwidth of 1.0734 THz and a sidelobe suppression of 19.79 dB. In addition, a low insertion loss of <0.6 dB and a low in-band ripple of less than 0.2 dB were obtained. The filter has a compact device footprint of 380 μm^2.

1. Introduction

Optical filters are essential components in modern optical communication systems and sensing applications. To meet the ever-increasing demands for wideband applications, such as coarse wavelength division multiplexing (CWDM) [1,2], dispersion engineering [3], and others, a filter with a flat band is essential. Especially for WDM systems, the ever-increasing demand for broadband access in data centers and high-performance computing systems need high-performance filters [4]. Also, such wideband filters (WBF) must be implemented in a small chip area. Therefore, silicon-based photonics filters, which are compatible with complementary metal-oxide-semiconductor (CMOS) technology, are considered an excellent choice for realizing high-performance filtering. Besides, silicon-based techniques provide compact size, low cost, robustness, and large-scale integration. Several researchers have demonstrated silicon-based photonic filters using Mach-Zehnder interferometer (MZI) [5], Bragg grating [6], microring resonators (MRRs) [7–10], arrayed-waveguide gratings [11], and contradirectional coupler [12]. Among those devices, filters based on MRR recently attracted many interests because of their compact size and flexibility in their functions. Large bandwidth (BW), wide free spectral range (FSR), and flat-top response are required for multiplexing/de-multiplexing to meet the demand of WDM-based links. Hence, the conventional MRR, which gives a Lorentzian shape with very sharp peaks, is unsuitable for broadband filtering. Numerous researchers have developed various filters based on MRR with different configurations [13,14]. In [13], a flat-top response is achieved by using four two-stage cascaded MRRs that has a maximum passband width of 300 GHz and a good shape factor (SF) of >0.2 (the ratio between the −1 dB and −10 dB bandwidth), but it has a

#448715 https://doi.org/10.1364/OPTCON.448715
Journal © 2022 Received 17 Nov 2021; revised 13 Jan 2022; accepted 19 Feb 2022; published 16 Mar 2022

OPTICS CONTINUUM

high insertion loss (IL) of ~4 dB. In [14], a flat-top filter is proposed with five cascaded MRRs, which shows a maximum passband width of 125GHz and an IL of 0.5dB but has a large ripple. Although cascaded MRRs can obtain a relatively good filtering performance, the footprint issue is challenging with an increase in the order of MRR. A filter based on combining the MRR and MZI was demonstrated in [15] with a flat top response and a maximum bandwidth of 173 GHz, but it has a limited FSR (maximum value is 25 GHz). All the WBF mentioned above are based on MRR and use multiple MRRs. Hence, in this work, we propose a new design technique that uses a single MRR to demonstrate a WBF that provides low IL, high FSR, and a small footprint.

In this paper, we propose a wideband filter based on a novel structure of double modulated grating-assisted MRR on a silicon-on-insulator (SOI) platform to provide a wide band, high sidelobe suppression, FSR-free response, and a compact size. The proposed scheme consists of a waveguide and a single MRR ring with double modulated grating-assisted MRR. In the design, the waveguide formed by Bragg grating is adopted [16]; as a result, there is only one prominent peak and no FSR [16]. For the MRR ring, a new structure of Bragg grating is proposed. The proposed Bragg grating structure in the MRR consists of a subwavelength grating (SWG) waveguide with two gratings of the same period but with different fill factors. Different fill factors with the same periods induce variation in refractive index along the direction of the propagation, causing double modulation of the signal. With proper selection of the design parameters, the double modulation can be coupled, providing a wider bandwidth. In addition, in our proposed design, the combined effect of the double modulated grating-assisted MRR and waveguide grating coupling suppress the sidelobe significantly. In our design, silica is chosen as upper cladding, a protective layer for the SWG. A taper in the straight waveguide is adapted to couple the mode between the strip and SWG waveguide [17]. A flat-top response with a 3dB bandwidth of 1.0734 THz and 1.0750 THz at the passband and stopband, respectively, are demonstrated through our proposed WBF with a double modulated grating-assisted MRR. Furthermore, an IL of less than 0.6 dB, an in-band ripple of <0.2 dB, and SF of 0.44 at the in-port (input port) are observed. The proposed scheme uses only a single MRR of 5 μm radius; thus, a small device footprint of about 380 μm^2 (35×10.857) is obtained. Hence, the proposed device is promising for optical communication systems, where wide bandwidth and a small footprint are essential.

2. Device structure and operation

The schematic diagram of the proposed ultra-compact WBF is illustrated in Fig. 1. The proposed structure uses an SOI wafer with a 0.22 μm thick silicon layer, 2 μm thick buried oxide layer, and an extra 2 μm thick silicon dioxide cladding to protect the device from environmental interference. The proposed device structure mainly consists of a waveguide and the MRR. The device structure is divided into four regions, as illustrated in Fig. 1(a). The waveguide comprises tapered SWG (Region I and II) and SWG (Region III) and an MRR ring (Region IV), which consists of a new structure of double modulated SWG. The tapered SWG converts a conventional waveguide mode propagating in a silicon strip into a Bloch mode in the SWG waveguide and vice versa, making the device compatible with other devices on the chip. The parameters of the taper waveguides, sections I and II, are represented as follows: the width of the strip waveguide and the start of the taper is W_1; the end of the taper (end-width) is W_2; the period and fill factor of the SWG taper are Λ_t and D_t, respectively; and the length of the taper is L_{taper}. The width of the taper varies linearly from W_1 to W_2 over the length, L_{taper}, as shown in Fig. 1(b). Region III comprises the SWG waveguide, which comes immediately after the SWG taper, Region I. The width of the SWG waveguide is the same as that of the strip waveguide, W_1. The period, fill factor, and length of the SWG waveguide are Λ_c, D_c and L_c, respectively, as shown in the inset of Fig. 1(b). Region IV is the MRR ring with a radius of R. The MRR ring comprises a novel structure of a double modulated SWG waveguide with different fill factors ($f_1 \neq f_2$) but with the same periods ($\Lambda_{SWG1} = \Lambda_{SWG2}$) unlike in the conventional SWG MRR with a single period and fill factor. The

OPTICS CONTINUUM

fill factor refers to the ratio of silicon to the period of the SWG. The width and the gap between the MRR ring and SWG waveguide of the proposed structure is W_R, and G, respectively.

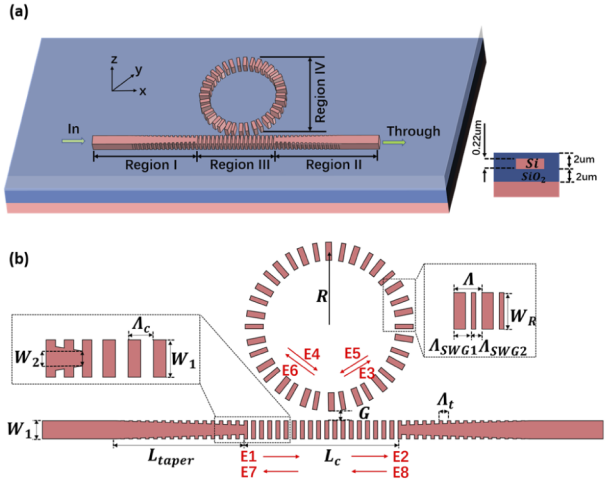

Fig. 1. Schematic diagrams of the proposed double modulated grating assisted MRR with design parameters labeled: (a) Three-dimensional perspective view. (b) Two-dimensional top view.

In the proposed scheme, a new structure of the Bragg grating with two SWG waveguides with the same period but different fill factors are used to enlarge the FSR and significant sidelobe suppression. When the Bragg reflection occurs at one of the resonance wavelengths of the MRR, the other side modes of the MRR are suppressed due to the vernier effect [16]. As a result, the FSR can be large enough and considered infinite compared to conventional MRRs and single modulated SWG MRRs, whose FSRs are limited by radius [18]. With the proposed structure, not only can we achieve the flat-top amplitude response of the Bragg grating for the MRR. The double modulated gratings give two different resonant peaks for different fill factors. The coupling of these resonant modes, which can be obtained by the proper selection of the parameters of the structure, provides the flat-top response. The higher side mode suppression is achieved due to the combined effect of the double-modulated grating-assisted MRR and the grating coupled MRR, and Bragg reflection coincides with one of the resonance wavelengths of the MRR. For the MRR, the resonance wavelength can be expressed as follows [19]:

$$n\lambda_{MRR} = n_{eff}L\,, \tag{1}$$

where λ_{MRR} is the resonance wavelength of MRR, n is an integer, n_{eff} is the equivalent effective refractive index of the ring waveguide, and L is the circumference of the MRR.

For Bragg grating, the first-order Bragg wavelength is given as:

$$\lambda_{Bragg} = 2\Lambda_{Bragg}n_{eff}, \tag{2}$$

where λ_{Bragg} is Bragg reflection wavelength, Λ_{Bragg} is the period of Bragg grating ($\Lambda = \Lambda_{SWG1} + \Lambda_{SWG2}$). To attain higher FSR, λ_{Bragg} and λ_{MRR} should be identical. Therefore, the circumference of the MRR ring, $L = 2n\Lambda_{Bragg}$, which is obtained by combining (1) and (2), also shows that the number of a period should be even. Also, it should be noted that all the SWG waveguides (including SWG1 and SWG2) are set to work in subwavelength operation regimes [20].

The transmission and reflection of the proposed device are calculated by using the transfer matrix method. Each period of Bragg grating comprises SWG1 and SWG2 with an effective

OPTICS CONTINUUM

index of n_{eff1} and n_{eff2}, and a loss coefficient of α_1 and α_2, respectively. The period of SWG1 and SWG2 are the same. The fill factor of SWG1 is made constant at 0.5, whereas the fill factor of SWG2 is varied. The effective index of SWG2 can be written as $n_{eff2} = n_{eff1} \pm \Delta n_{eff}(f_2)$, where n_{eff1} is the effective index of the SWG with a 0.5 fill factor, and $\Delta n_{eff}(f_2)$ is a change in the refractive index due to change in the fill factor. We consider both SWGs with different fill factors as homogeneous, and thus the transfer matrix can be expressed as follows [21]:

$$T_{SWGi} = \begin{bmatrix} e^{j\beta_i \Lambda_{SWGi}} & 0 \\ 0 & e^{-j\beta_i \Lambda_{SWGi}} \end{bmatrix}, \tag{3}$$

where i = 1 or 2 to represent the SWG1 or SWG2, β_i is the propagation constant of the equivalent waveguide of SWG1 or SWG2 and given by $\beta_i = \frac{2\pi n_{effi}}{\lambda} - j\alpha_i$. At the interface of the SWG waveguide of the ring, the transfer matrix can be expressed as [22]:

$$T_{SWGi-SWGj} = \begin{bmatrix} \frac{n_{effi}+n_{effj}}{\sqrt{n_{effi}n_{effj}}} & \frac{n_{effi}-n_{effj}}{\sqrt{n_{effi}n_{effj}}} \\ \frac{n_{effi}-n_{effj}}{\sqrt{n_{effi}n_{effj}}} & \frac{n_{effi}+n_{effj}}{\sqrt{n_{effi}n_{effj}}} \end{bmatrix}, \tag{4}$$

where $i, j = 1\ or\ 2$ and $i \neq j$. The transfer matrix for Bragg grating with N numbers of the period is shown as follows:

$$\begin{aligned} T_{Bragg,\,N} &= (T_{SWG1} \cdot T_{SWG1-SWG2} \cdot T_{SWG2} \cdot T_{SWG2-SWG1})^N \\ &= \begin{bmatrix} T_{11} & T_{12} \\ T_{21} & T_{22} \end{bmatrix}, \end{aligned} \tag{5}$$

where T_{11}, T_{12}, T_{21} and T_{22} are the elements of the $T_{Bragg,\ N}$. For Bragg grating, the relationships between electrical field E_3 , E_4 , E_5 and E_6 , as shown in Fig. 1(b), can be expressed as follows:

$$\begin{bmatrix} E_4 \\ E_6 \end{bmatrix} = T_{Bragg,N} \begin{bmatrix} E_3 \\ E_5 \end{bmatrix}. \tag{6}$$

At the interface of the coupling region of the MRR ring and SWG waveguide, the relationship can be described by [23]:

$$\begin{bmatrix} E_2 \\ E_3 \end{bmatrix} = T_c \begin{bmatrix} E_1 \\ E_4 \end{bmatrix} \tag{7}$$

$$\begin{bmatrix} E_7 \\ E_6 \end{bmatrix} = T_c \begin{bmatrix} E_5 \\ E_8 \end{bmatrix}, \tag{8}$$

where $T_c = \begin{bmatrix} \tau & jk \\ jk & \tau \end{bmatrix}$ is coupling matrix, and τ and k are transmission and coupling coefficients, respectively. Here, $E_8 = 0$, hence, reflectance and transmittance amplitude response at the In

OPTICS CONTINUUM

port (input port) and Through port can be written as follows by combing (6), (7), and (8):

$$T = \left|\frac{E_2}{E_1}\right|^2 = \left|\frac{-1-k^2+k(T_{11}+T_{22})}{T_{22}-2k+k^2T_{11}}\right|^2 \tag{9}$$

$$R = \left|\frac{E_7}{E_1}\right|^2 = \left|\frac{(1-k^2)T_{21}}{T_{22}-2k+k^2T_{11}}\right|^2 . \tag{10}$$

With two fill factors $f_1 = 0.46$ and $f_2 = 0.54$, effective indexes $n_{eff1} = -0.0009\left(\frac{\lambda-1.5344}{92.3}\right)^3 + 0.0083\left(\frac{\lambda-1.5344}{92.3}\right)^2 - -0.062\left(\frac{\lambda-1.5344}{92.3}\right) + 1.4049$, $\Delta n_{eff}(f_2) = 1.0927(f_2 - 0.5275) + 0.0240$, $\alpha_i = 3$ dB/cm, $k = 0.32$, and $N = 58$, the transmittance and reflectance can be observed, as shown in Fig. 2, using (9) and (10). In Fig. 2, the two dips are seen due to two fill factors. These two resonant modes can be coupled with proper selection of MRR parameters to provide a flat top.

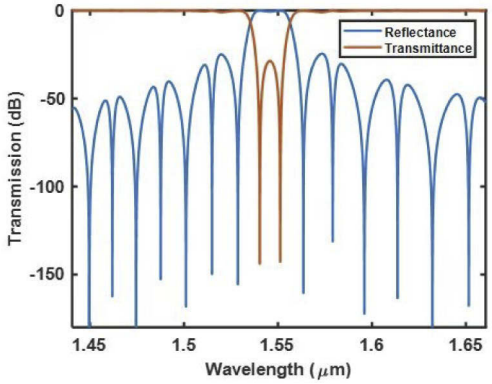

Fig. 2. Transmittance and Reflectance of double modulated MRR

3. Simulation results

All design parameters for the simulation of the proposed ultra-compact WBF are shown in Fig. 1. To show that our chosen design parameters were optimized for desired performance, we illustrate the design process for the waveguide, waveguide with MRR ring, and our optimized structure. At first, we analyze the waveguide design. Considering the Bloch mode propagating in the SWG waveguide of the MRR ring and the light mode propagating in the strip waveguide is essentially different, two tapers, one at the beginning (input) and another at the end (output), are designed to reduce the additional power losses. The strip waveguide connected to the taper act as an interface from other devices. The width, W_1, of the strip waveguide is chosen to be 0.45 μm, so that the device works as a single mode for transverse electric (TE) polarization at 1.55 μm, as shown in Fig. 3(a). To reduce the power losses substantially, which are caused by the mode conversion between the strip and SWG waveguide, the length, L_{taper}, and the W_2 is set at 15 μm and 0.2 μm, respectively. Also, Λ_t and D_t are set at 0.2 μm and 0.5, respectively. Depending on the period and duty cycle of the SWG waveguide, three different working regimes can be achieved: diffraction regime, reflection regime, and subwavelength regime. Negligible power loss is achieved only when the SWG waveguide's operating wavelength range lies within the subwavelength regime. Hence, all the structures related to SWG waveguide, including the SWG waveguide in Region III and Bragg grating in Region IV, are selected to be in working wavelengths of the subwavelength regime in the design. For this purpose, the period Λ_c and D_c are chosen to be 0.275 μm, and 0.5,

OPTICS CONTINUUM

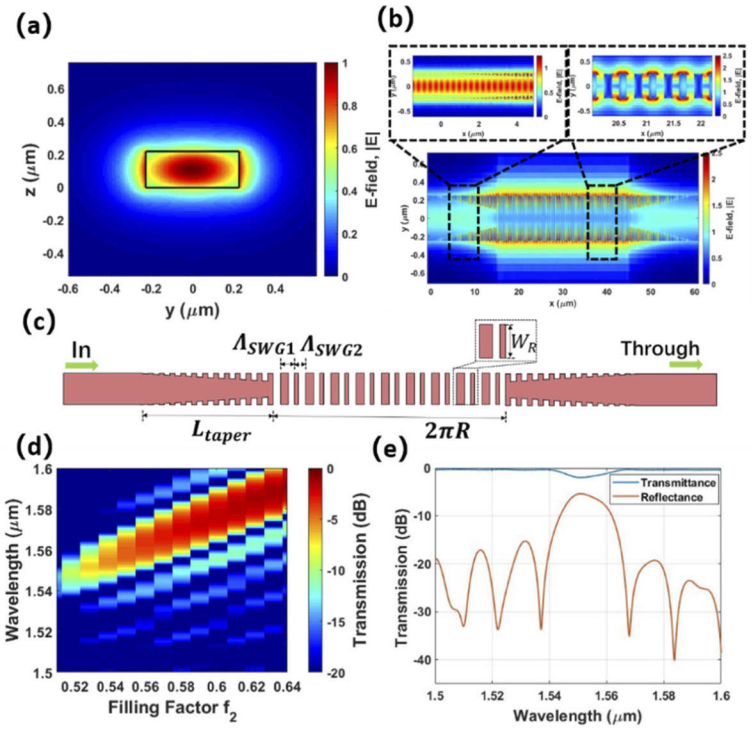

Fig. 3. (a) E-field distribution of strip waveguide at 1.55 μm wavelength. (b) E-field distribution of Bloch mode propagating in Region I, II, and III. (c) Schematic of double modulated Bragg grating waveguide. (d) Reflectance response of Bragg grating versus wavelength versus fill factor f_2 . (e) Transmission response of Bragg grating with $f_1 = 0.5$ and $f_2 = 0.54$.

respectively. In Fig. 3(b), a Bloch mode propagation is observed because Regions I, II, and III are selected in such a way that they work in the subwavelength regime, as shown in Fig. 3(b).

Next, we investigate the Bragg waveguide consisting of two SWGs with the same periods but different fill factors, as illustrated in Fig. 3(c). The fill factor of one SWG is kept constant at 0.5, whereas that of another is varied. The Ansys Lumerical 2.5D FDTD solver is used to analyze the variation of the Bragg wavelength with a change in the fill factor. The simulation parameters for the analysis of the waveguide are as follows: $W_R = 0.5$ μm; $f_1 = 0.5$; $\Lambda_{SWG1} = \Lambda_{SWG2} = 0.275$ μm; the length of the Bragg grating is equal to $2\pi R$, where $R = 5$ μm. Figure 3(d) shows the change in the Bragg wavelength with a different fill factor of SWG2. This analysis is used as a reference for designing a double modulated SWG MRR ring for a particular wavelength. Also, we observed that with an increase in the fill factor f_2 , the bandwidth increases. For the wavelength of 1.55 μm, the fill factor, $f_2 = 0.54$ is observed. Since we are focused on the communication band, we analyzed the transmission and reflection response of Bragg grating at 1.55 μm, which is shown in Fig. 3(e). High ripples are observed in the reflectance, whereas no stopband is observed at the transmittance response.

Further, we analyze the waveguide with the MRR ring, as illustrated in Fig. 4 that has a cladding layer of the same thickness as shown in Fig. 1(a). All the parameters of the straight waveguide are kept the same as that in Fig. 1. The MRR ring has a 5 μm radius, 0.5 μm width, 275 nm period, and a fill factor of 0.5, which are the same as SWG1 used in Bragg grating. The coupling gap between the waveguide and the MRR ring is 0.65 μm. The transmittance

OPTICS CONTINUUM

and reflectance response of the structure in Fig. 4(a) are shown in Fig. 4(b). The Through port shows that maximum power is transferred to output with an FSR of ~31 nm, a Lorentzian shape, and very narrow bandwidth. Figure 3(c) shows the effect of change in the fill factor in the transmittance response. The shift in transmittance wavelength is observed with a change in fill factor, whereas only a small change in the FSR and the bandwidth.

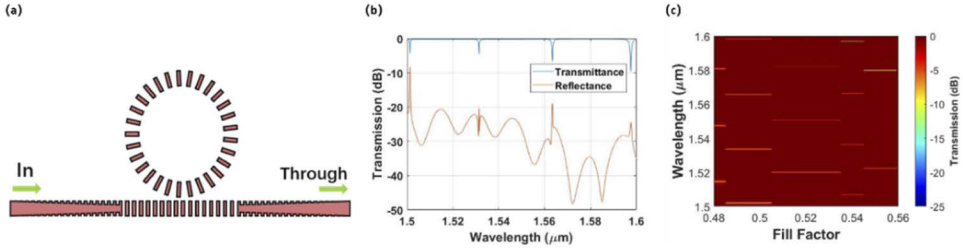

Fig. 4. (a) Schematic of SWG MRR with a single period on a ring and the bus waveguide. (b) Transmittance and reflectance response (c) Transmittance response with change in fill factor

By observing Fig. 3 and Fig. 4, it is clear that the SWG waveguide can be chosen so that wide bandwidth can be obtained, and with the use of the SWG MRR ring, ripples can be reduced significantly. Therefore, we propose a new structure for the WBF by modifying the structure of Fig. 4. We introduce a double fill factor in a Bragg period of the MRR ring in the proposed structure, as illustrated in Fig. 1. Ansys Lumerical FDTD is used with extra mesh to analyze the proposed design. For the MRR ring and tapers in Region I and II, the mesh size is set at 10 nm in both the x- and y-direction, and for the SWG waveguide in Region III, the mesh is set at 5 nm. The perfect matching layer (PML) boundary condition is set in all the simulation regions. Furthermore, the distance between the PML boundary and the device is set to be more than half of the maximum simulated wavelength. Also, the long simulation time is chosen to sufficiently attenuate the electromagnetic field in the simulation region. The parameters for the proposed structure are: $W_1 = 0.45$ μm, $W_2 = 0.2$ μm, $L_{taper} = 15$ μm, $\Lambda_{\text{Bragg}} = 0.55$ μm, $\Lambda_{SWG1} = \Lambda_{swg2} = 0.275$ um, $f_1 = 0.5$, and $W_R = 0.5$ μm. It should be noted that the asymmetry waveguide width, W_1 and W_R, are chosen to obtain the best output sidelobe suppression, wide bandwidth response, and single mode in strip waveguide [16].

Figure 5 illustrates the response of the proposed structure of double modulated MRR WBF. The effect of the fill factor of SWG2 on the center wavelength of the filter is shown in Fig. 5(a). With an increase in the fill factor of SWG2, the effective refractive index of the device increases. Hence, a linear redshift in the center resonance frequency is observed. Also, we observe the increase in the bandwidth with increasing f_2. By using the curve fitting results from 2.5D FDTD, the effective refractive index $n_{eff1} = -0.0009\left(\frac{\lambda-1.55344}{92.3}\right)^3 + 0.0083\left(\frac{\lambda-1.55344}{92.3}\right)^2 - 0.062\left(\frac{\lambda-1.55344}{92.3}\right)^2$, and the $\Delta n_{\text{eff}}(f_2) = 0.018\, f_2 + 0.0142$ [24]. The coupling coefficient is fixed at 0.3 in the calculation. The center wavelength obtained from the reflection using Eq. (10) is indicated with a dashed white line in Fig. 5(a). It is clear from Fig. 5(a) that the calculated center wavelength of the structure is matched with that of the simulation results for various fill factor f_2. To observe the filter response with center frequency 1545 nm, the 0.54 fill factor of SWG2 is chosen. Figure 5(b) shows the transmission at input wavelength versus gap, G. The coupling coefficient changes as we change the gap between the MRR ring and the waveguide. Figure 5(b) shows that a relatively better flatness is achieved when the gap equals 0.35 μm.

The filter's response and the electric field profile at 1.545 μm wavelength with a gap, G = 0.35 μm, are shown in Fig. 5(c) and (d), respectively. Figure 5(c) shows a flat-top bandpass response with 1.0734 THz bandwidth, 0.52 dB IL, and 19.79 dB sidelobe suppression is achieved

OPTICS CONTINUUM

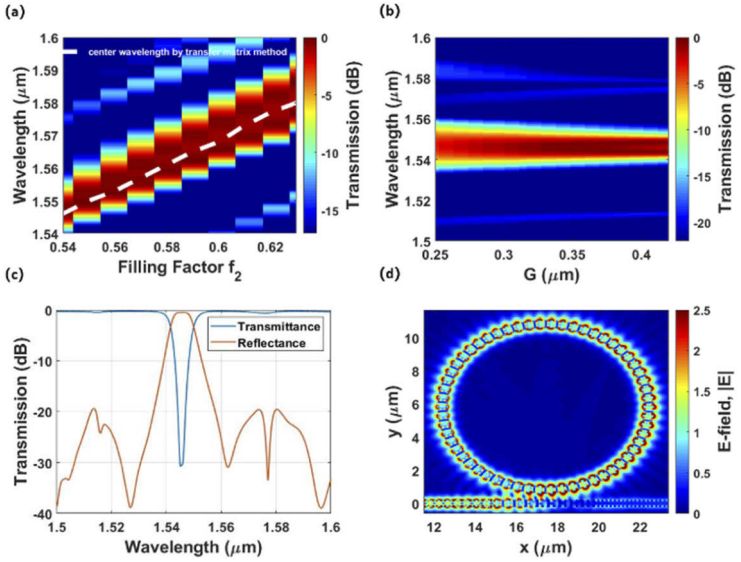

Fig. 5. (a) Reflectance versus wavelength versus fill factor f_2 . (b) Reflectance versus wavelength versus gap G . (c) Transmission response of the device with gap G = 0.35 μm . (d) E-field distribution of the device at 1.545 μm wavelength showing the coupling of light to the MRR

at reflectance. The SF is 0.44, and the reflectance ripple is lower than 0.2 dB. A bandstop response is observed at the Through port with an extinction ratio over 30 dB, no FSR, and bandwidth of 1.0750 THz. To further investigate the effect of the variation of both fill factors (f_1 *and* f_2), f_1 is kept constant at 0.45 and f_2 is varied from 0.51 to 0.6 with the step of 0.1 at first and later repeated the same for different f_1 (0.5 and 0.55), while changing the fill factor, f_2 . The reflectance response at the In port is presented in Table 1 and shows the change in the center wavelength and the bandwidth. Table 1 shows that the proposed structure of double modulated WBF can be tuned to a wide range of center wavelength and bandwidth by changing the fill factor. Since both SWGs' period is the same, setting the fill factor of either SWG1 or SWG2 constant and varying the other or vice-versa has no effect on the output response.

Table 1. Bandwidth and center wavelength for different fill factors f_1 and f_2

f_2	Bandwidth (THz)			Center wavelength (μm)		
	f_1 = 0.45	f_1 =0.5	f_1 =0.55	f_1 = 0.45	f_1 =0.5	f_1 =0.55
0.51	2	0.5	0.9625	1.515	1.534	1.552
0.52	2.2	0.6625	0.70375	1.539	1.538	1.556
0.53	2.3625	0.8625	0.52375	1.523	1.542	1.559
0.54	2.5375	1.075	0.45	1.527	1.545	1.563
0.55	2.6875	1.2625	/	1.532	1.549	/
0.56	2.8	1.4375	0.38125	1.535	1.553	1.571
0.57	2.9125	1.5875	0.44125	1.539	1.557	1.575
0.58	3.013	1.7	0.595	1.542	1.560	1.579
0.59	3.075	1.8125	0.7	1.547	1.565	1.583
0.60	3.125	1.825	0.845	1.55	1.569	1.587

OPTICS CONTINUUM

4. Conclusion

In conclusion, we proposed and demonstrated a new structure, double modulated SWG MRR, for a wideband, high sidelobe suppression, and a flat-top filter. Double modulation is obtained using two SWG in the MRR with different fill factors but the same period. Unlike in other designs of WBF based on MRRs, where either multiple MRRs are cascaded or used MRR and waveguide to obtain a wideband flat-top filter, our proposed structure used only one microring without any other waveguides. By appropriately choosing the device's parameters, we obtain a 3-dB bandwidth of 1.0625 THz, IL of 0.6 dB, a reflectance ripple of less than 1 dB, free from FSR, and a small fabrication footprint of 380 μm^2. The minimum feature of our device is 100 nm, which makes it possible to be fabricated by electron beam lithography and is in consideration for fabrication as future work and to carry out further experimental analysis of the output performance of the proposed WBF. Given the output performances of the proposed device, it is suitable for the application of CWDM and other broadband applications.

Funding. Nanjing University of Aeronautics and Astronautics (90YAH21066); Nazarbayev University (021220FD0451).

Disclosures. The authors declare no conflicts of interest.

Data availability. Data underlying the results presented in this paper are not publicly available at this time but may be obtained from the authors upon reasonable request.

References

1. K. Iwatsuki, J. Kani, H. Suzuki, and M. Fujiwara, "Access and Metro Networks Based on WDM Technologies," J. Lightwave Technol. **22**(11), 2623–2630 (2004).
2. J. Kani, M. Teshima, K. Akimoto, N. Takachio, H. Suzuki, and K. Iwatsuki, "A WDM-based optical access network for wide-area gigabit access services," IEEE Commun. Mag. **41**(2), 77–82 (2003).
3. A. D. Simard and S. LaRochelle, "Complex apodized Bragg grating filters without circulators in silicon-on-insulator," Opt. Express **23**(13), 16662–16675 (2015).
4. M. Teshima, M. Fujiwara, J. Kani, H. Suzuki, M. Amemiya, N. Takachio, and K. Iwatsuki, "Optical carrier supply module applicable to over 100 super-dense WDM systems of 1000 channels," in *Proceedings 27th European Conference on Optical Communication* (2001) 98–99.
5. F. Horst, W. MJ Green, S. Assefa, S. M. Shank, Y. A. Vlasov, and B. Jan Offrein, "Cascaded Mach-Zehnder wavelength filters in silicon photonics for low loss and flat passband WDM, (de-)multiplexing," Opt. Express **21**(10), 11652–11658 (2013).
6. J. Jiang, H. Qiu, G. Wang, Y. Li, T. Dai, X. Wang, H. Yu, J. Yang, and X. Jiang, "Broadband tunable filter based on the loop of multimode Bragg grating," Opt. Express **26**(1), 559–566 (2018).
7. W. Bogaerts, P. De Heyn, T. Van Vaerenbergh, K. De Vos, S. Kumar Selvaraja, T. Claes, P. Dumon, P. Bienstman, D. Van Thourhout, and R. Baets, "Silicon microring resonators," Laser Photonics Rev. **6**(1), 47–73 (2012).
8. A. M. Prabhu, A. Tsay, Z. Han, and V. Van, "Ultracompact SOI Microring Add–Drop Filter with Wide Bandwidth and Wide FSR," IEEE Photonics Technol. Lett. **21**(10), 651–653 (2009).
9. S. Pan, Z. Tang, M. Huang, and S. Li, "Reflective-Type Microring Resonator for On-Chip Reconfigurable Microwave Photonic Systems," IEEE J. Sel. Top. Quantum Electron. **26**(5), 1–12 (2020).
10. N. Eid, R. Boeck, H. Jayatilleka, L. Chrostowski, W. Shi, and N. A. F. Jaeger, "FSR-free silicon-on-insulator microring resonator based filter with bent contra-directional couplers," Opt. Express **24**(25), 29009–29021 (2016).
11. J. Zou, X. Xia, G. Chen, T. Lang, and J. J. He, "Birefringence compensated silicon nanowire arrayed waveguide grating for CWDM optical interconnects," Opt. Lett. **39**(7), 1834–1837 (2014).
12. B. Liu, Y. Zhang, Y. He, X. Jiang, J. Peng, C. Qiu, and Y. Su, "Silicon photonic bandpass filter based on apodized subwavelength grating with high suppression ratio and short coupling length," Opt. Express **25**(10), 11359–11364 (2017).
13. T. Dai, G. Wang, X. Guo, C. Bei, J. Jiang, and W. Chen, "Scalable Bandwidth-Tunable Micro-Ring Filter Based on Multi-Channel-Spectrum Combination," IEEE Photonics Technol. Lett. **30**(11), 1044–1047 (2018).
14. J. R. Ong, R. Kumar, and S. Mookherjea, "Ultra-High-Contrast and Tunable-Bandwidth Filter Using Cascaded High-Order Silicon Microring Filters, in *IEEE Photonics Technology Letters* 25 (2013) 1543–1546.
15. P. Orlandi, C. Ferrari, M. J. Strain, A. Canciamilla, F. Morichetti, M. Sorel, P. Bassi, and A. Melloni, "Reconfigurable silicon filter with continuous bandwidth tunability," Opt. Lett. **37**(17), 3669–3671 (2012).
16. W. Shi, X. Wang, W. Zhang, H. Yun, C. Lin, L. Chrostowski, and N. A. F. Jaeger, "Grating-coupled silicon microring resonators," Appl. Phys. Lett. **100**(12), 121118 (2012).
17. J. Wang, I. Glesk, and L. R. Chen, "Subwavelength grating filtering devices," Opt. Express **22**(13), 15335–15345 (2014).
18. V. Donzella, A. Sherwali, J. Flueckiger, S. M. Grist, S. T. Fard, and L. Chrostowski, "Design and fabrication of SOI micro-ring resonators based on sub-wavelength grating waveguides," Opt. Express **23**(4), 4791–4803 (2015).

OPTICS CONTINUUM

19. I. Teraoka, "A hybrid filter of Bragg grating and ring resonator," Opt. Commun. **339**, 108–114 (2015).
20. R. Halir, P. J. Bock, P. Cheben, A. Ortega-Moñux, C. Alonso-Ramos, J. H. Schmid, J. Lapointe, X. Dan-Xia, J. Gonzalo Wangüemer-Pérez, Í. Molina-Fernández, and S. Janz, "Waveguide sub-wavelength structures: a review of principles and applications," Laser Photonics Rev. **9**(1), 25–49 (2015).
21. L. A. Coldren, S. W. Corzine, and M. L. Mashanovitch, *Diode Lasers and Photonic Integrated Circuits*, 2nd ed., John Wiley & Sons, 2012.
22. L. Chrostowski and M. Hochberg, *Silicon photonics design*, Cambridge University Press, 2015
23. J. K. S. Poon, J. Scheuer, S. Mookherjea, G. T. Paloczi, Y. Huang, and A. Yariv, "Matrix analysis of microring coupled-resonator optical waveguides," Opt. Express **12**(1), 90–103 (2004).
24. https://www.lumerical.com/learn/video/swg-bandstructures/